



POLITECNICO
MILANO 1863

GOATS mission Spacecraft Attitude Dynamics



Group 75
Project 721

Enis Arikan 10775709
Aerospace Engineering METU
Riccardo Siri 10531042
Aerospace Engineering POLIMI

Gianluca Lardo 10482528
Aerospace Engineering POLIMI
Alessandro Stabile 10561985
Aerospace Engineering POLIMI

Final Report

Course of Spacecraft Attitude Dynamics and Control
School of Industrial Engineering
Academic Year 2022-2023

Abstract

The purpose of this report is the conceptual design of an attitude control system, starting from certain specifications. According to those, the geostationary telecommunication satellite Amos-3 has been chosen as a baseline. The mass, orbit, and purpose of the mission, in the following system design and the baseline one, are similar. The main objective will be to de-tumble the spacecraft, starting with certain initial angular speeds conditions, then to manoeuvre the satellite to point a specific region of the Earth, and finally to perform tracking in that position. Below are the specifications and the adjustments that have been done:

Table 1: Project Specifications

	Specification	Modifications	Motivation
Platform	Large Satellite	-	-
Attitude Parameters	Quaternions	-	-
Mandatory Sensors	Gyroscopes	Star Sensor	Precision Tracking and Redundancy
Actuators	Reaction Wheels (3)	Thrusters	Desaturation and Redundancy

Contents

1	Introduction	1
1.1	Operational Context	1
1.2	Satellite Configuration	2
1.3	Design guidelines	3
2	Model Implementation	4
2.1	Dynamics	4
2.2	Kinematics	4
2.3	Attitude Matrices	4
2.4	Simulink Model	5
3	Environment Perturbations	6
3.1	Gravity Gradient	6
3.2	Solar Radiation Pressure	6
3.2.1	Umbra and Penumbra	7
3.3	Magnetic Perturbation	7
3.4	Disturbance Torques	8
4	Sensors	10
4.1	Gyroscopes	10
4.2	Star Sensor	11
4.2.1	Star Selection	11
4.3	Wahba Attitude Reconstruction	11
5	Control	12
5.1	Lyapunov Controller	12
6	Actuators	13
6.1	Reaction Wheels	13
6.2	Thrusters	15
7	Results	16
7.1	De-tumbling	16
7.2	Slew Manoeuvre	16
7.3	Tracking	16
7.4	Comments on Computational Cost	16
8	Conclusions	17
A	<i>Solar panel mass and area computation</i>	18
B	<i>Results with thrusters on</i>	19

List of Figures

1.1	GOATS geostationary orbit	1
1.2	GOATS structural model	2
2.1	Simulink model divided in subsystems	5
3.1	Shadow Geometry	7
3.2	Disturbance torques by component	8
3.3	Disturbance torques by type	9
6.1	Actuator torque for RWs	14
6.2	Angular momentum for RWs	14
6.3	Angular velocities with RWs on	15
B.1	Angular velocities with thrusters on	19
B.2	Angular velocities with thrusters on	20
B.3	Manual Switch to select actuators for the simulation	21

List of Tables

1	Project Specifications	i
1.1	Geostationary orbit parameters	2
1.2	GOAT Satellite main body configuration	2
3.1	Magnetic Model Constants	7
4.1	Gyroscope Specifications [1]	10
4.2	Star Sensor Specifications	11
5.1	Controller weights	12
6.1	Reaction Wheel Specifications	13
A.1	Mass and Area of the solar panel result	18

Nomenclature

Acronyms and Abbreviations		
<i>ARW</i>	Angular Random Walk	\hat{n} Normal to Surface
<i>BOL</i>	Begining-of-life	P Solar Pressure at 1AU [W/m^2]
<i>DET</i>	Direct Energy Transfer	\underline{q} Quaternions
<i>EOL</i>	End-of-life	r Distance from Earth to S/C [m]
<i>FOV</i>	Field of View	\hat{S} Sun-Earth versor
<i>GG</i>	Gravity Gradient	\hat{s}_b S/C - Sun versor in Body frame
<i>LVLH</i>	Local-Vertical-Local-Horizontal	\underline{T} External Torque [Nm]
<i>MAG</i>	Magnetic Perturbation	w Width (along y axis) [m]
<i>RRW</i>	Rate Random Walk	σ Variance [arcsec]
<i>RW</i>	Reaction Wheel	ρ_d Diffusive Reflectivity Coefficient
<i>S/C</i>	Spacecraft	ρ_s Specular Reflectivity Coefficient
<i>SRP</i>	Solar Radiation Pressure	μ Planetary Constant [km^3/s^2]
Constants and Variables		$\underline{\omega}$ Angular velocity [rad/s]
A	Area [m^2]	Keplerian Parameters
\underline{A}	Attitude Matrix	a Semi-major axis [km]
\underline{B}	Magnetic Field [T]	e Eccentricity
d	Depth (along x axis) [m]	i Inclination [°]
f	Frequency [Hz]	Ω RAAN [°]
h	Height (along z axis) [m]	ω Argument of Perigee [°]
\underline{h}	Angular Momentum [kgm/s^2]	θ True Anomaly [°]
\underline{I}	Identity Matrix	Subscripts and Superscripts
I	Inertia Component [kgm^2]	\oplus Earth
\underline{J}	Inertia Matrix [kgm^2]	B/L from LVLH to Body frame
\underline{k}	Controller Modes Matrix	B/N from Inertia to Body frame
l	Length [m]	CM Center of Mass
m	Mass [kg]	err Error

id	Ideal
L/N	from Inertia to LVLH frame
mb	Main Body
meas	Measured
req	Required
sat	Saturation
sa	Solar Array
SS	Star Sensor
s	Measured Star position
T	Thrusters

1. Introduction

The purpose of this report is to describe the design of the attitude control subsystem for a satellite, starting from the given specifications reported in Table 1. The design will be deeply analysed, highlighting the design choices, the models adopted, and the assumptions made during the development of the project.

1.1 Operational Context

In this section, a brief overview of the platform and its operational context are presented. The GOATS mission is performed by means of a large-class telecommunication satellite placed in a geostationary orbit, which characteristics are shown in Table 1.1. The attitude control system shall be capable to perform the three main manoeuvres listed below with a certain level of pointing accuracy:

- **De-tumbling:** the satellite shall be capable to stop its rotational motion after the detachment from the launcher.
- **Slew manoeuvre:** the satellite shall be capable to point a desired target starting from a condition of null rotational motion.
- **Tracking:** the satellite shall be capable to maintain the pointing of the target.

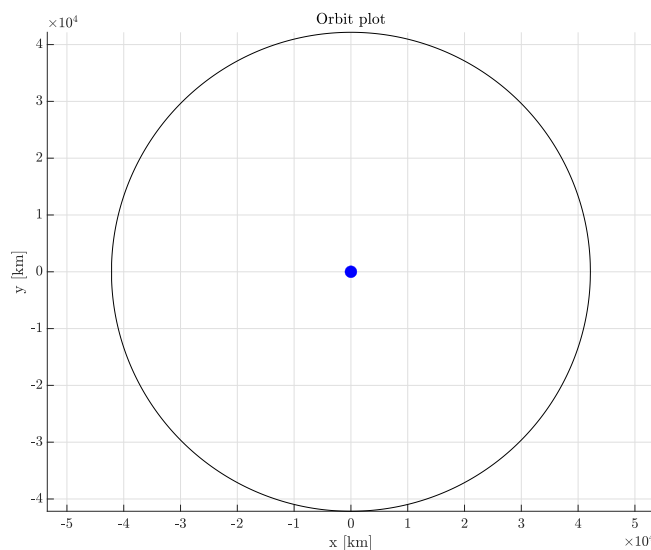


Figure 1.1: GOATS geostationary orbit

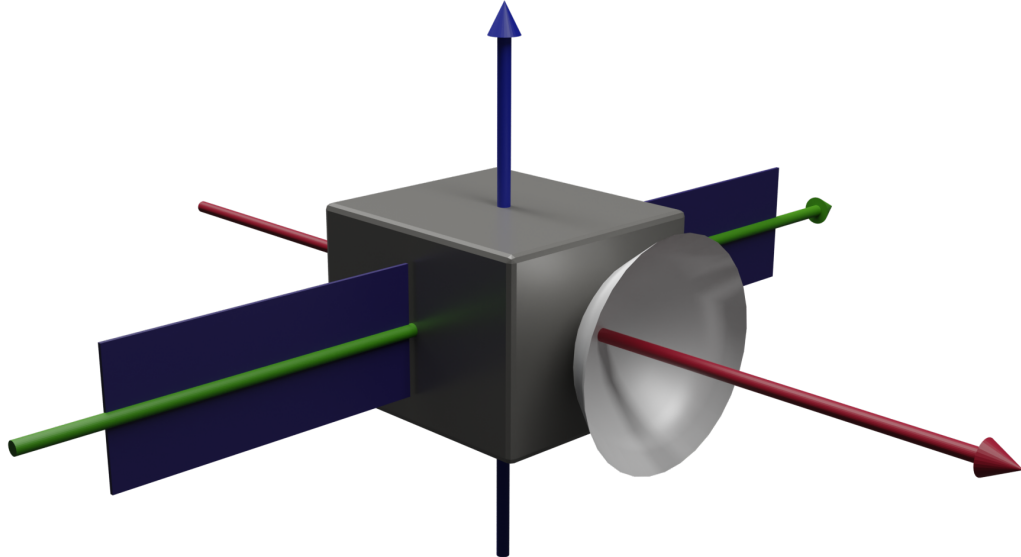
Table 1.1: Geostationary orbit parameters

a	e	i	Ω	ω	θ
[km]	-	[°]	[°]	[°]	[°]
42162	0	0	0	0	0

1.2 Satellite Configuration

The satellite configuration, in terms of mass and shape, has been chosen taking *AMOS-3* as a reference, an Israeli communications satellite operated by Spacecom Satellite Communications [4]. However, in order to obtain three different inertia values for the principal axes, the mass and the width of the main body of the spacecraft have been slightly modified. Data are shown in Table 1.2. Regarding the mass and the area of the solar panels, the computation has been performed starting from the nominal power requested by the S/C, esteemed with the algorithm displayed in appendix A.

The total inertia J of the satellite has been calculated by summing the contribution of the main body and the solar panels as reported below in Eq. (1.1). Assuming the mass of the spacecraft does not change during the mission, the inertia is constant over time and has been expressed in the principal axis reference frame to lower the computational burden due to coupling terms. In Fig. 1.2 the red line corresponds to the x axis, the green one corresponds to the y axis, the blue one corresponds to the z axis.

**Figure 1.2:** GOATS structural model**Table 1.2:** GOAT Satellite main body configuration

m_{mb}	m_{sa}	d_{mb}	h_{mb}	w_{mb}	d_{sa}	h_{sa}	w_{sa}
[kg]	[kg]	[m]	[m]	[m]	[m]	[m]	[m]
1186.43	13.57	2	1.5	1.8	0 ¹	1	2.4425

$$J = J_{mb} + J_{sa} \quad (1.1)$$

Here, J_{mb} and J_{sa} computation is reported below in Eq. (1.2).

$$J_{mb} = \begin{pmatrix} I_{xx,mb} & 0 & 0 \\ 0 & I_{yy,mb} & 0 \\ 0 & 0 & I_{zz,mb} \end{pmatrix}; \quad J_{sa} = \begin{pmatrix} I_{xx,sa} & 0 & 0 \\ 0 & I_{yy,sa} & 0 \\ 0 & 0 & I_{zz,sa} \end{pmatrix} \quad (1.2)$$

where the inertia moments have been calculated as follows in Eq. (1.3):

$$\begin{aligned} I_{xx,mb} &= \frac{m_{mb}}{12}(w_{mb}^2 + h_{mb}^2) \\ I_{yy,mb} &= \frac{m_{mb}}{12}(h_{mb}^2 + d_{mb}^2) \\ I_{zz,mb} &= \frac{m_{mb}}{12}(w_{mb}^2 + d_{mb}^2) \\ I_{xx,sa} &= \frac{m_{sa}}{12}w_{sa}^2 + \frac{m_{sa}}{12}\left(\frac{w_{sa}}{2} + \frac{w_{mb}}{2}\right)^2 \\ I_{yy,sa} &= \frac{m_{sa}}{12}h_{sa}^2 \\ I_{zz,sa} &= \frac{m_{sa}}{12}w_{sa}^2 + \frac{m_{sa}}{12}\left(\frac{w_{sa}}{2} + \frac{w_{mb}}{2}\right)^2 \end{aligned} \quad (1.3)$$

1.3 Design guidelines

In this section, the design guidelines adopted during the implementation are reported. First, the attitude dynamics of the spacecraft have been solved by integrating Euler's equations (chapter 2), including the most relevant sources of perturbation acting on the satellite: Solar Radiation Pressure (SRP), Gravity Gradient (GG) and Magnetic Perturbation (MAG) (chapter 3). Then, the attitude of the spacecraft has been retrieved from the dynamics, using quaternions as attitude parameters (chapter 2).

For the scope of this analysis, in order to focus the study on the rotational behavior of the spacecraft, the orbit propagation was performed according to the 2-body problem (Earth - S/C) without including the effect of perturbations, such as the J_2 effect, on the orbital elements. For this reason, the resulting motion of the spacecraft around the Earth is kept constant over time. Once the uncontrolled motion of the spacecraft has been defined, to fulfill the mission objectives, a set of gyroscopes and a star sensor have been equipped on the satellite in order to measure the current attitude (chapter 4).

Finally, a non-linear Lyapunov controller has been implemented (chapter 5) to gather and modulate the correct information and compute the required torque, which is applied by a set of actuators. These are reaction wheels and thrusters, mounted on the satellite to perform attitude manoeuvres (chapter 6).

¹Assuming 2D panels

2. Model Implementation

2.1 Dynamics

The rotational dynamics of the satellite is solved by integrating the Euler's equations, reported below in Eq. (2.1), in order to compute the time evolution of the angular velocities of the spacecraft.

$$J \frac{d\boldsymbol{\omega}(t)}{dt} = -\boldsymbol{\omega}(t) \times J\boldsymbol{\omega}(t) + \mathbf{T}(t); \quad (2.1)$$

\mathbf{T} includes the torques imposed by the different perturbations implemented, which are explained in detail in chapter 3, and the control torque applied by the actuators. The initial conditions selected for $\boldsymbol{\omega}$ are (0.05; 0.05; 0.1) rad/s, which are higher compared to residual angular velocities after launch indicated in Ariane 5 user's manual [2]. This to demonstrate that the attitude system works even in pessimistic scenarios.

2.2 Kinematics

First of all, it was necessary to express the orientation of the body frame with respect to the Earth-fixed inertial frame. **Quaternions** are used as the attitude parameter for kinematics. Eq. (2.2) shows the kinematics with this representation. The initial condition for the quaternions integration has been chosen as (0; 0; 0; 1).

$$\dot{\mathbf{q}} = \frac{1}{2}\Omega\mathbf{q}(t); \quad \begin{bmatrix} \dot{q}_1 \\ \dot{q}_2 \\ \dot{q}_3 \\ \dot{q}_4 \end{bmatrix} = \frac{1}{2} \begin{pmatrix} 0 & \omega_3 & -\omega_2 & \omega_1 \\ -\omega_3 & 0 & \omega_1 & \omega_2 \\ \omega_2 & -\omega_1 & 0 & \omega_3 \\ -\omega_1 & -\omega_2 & -\omega_3 & 0 \end{pmatrix} \begin{bmatrix} q_1 \\ q_2 \\ q_3 \\ q_4 \end{bmatrix}; \quad (2.2)$$

2.3 Attitude Matrices

Starting from quaternions, it is possible to reconstruct the attitude matrix $A_{B/N}$, to perform a frame change transformation from inertial frame to body frame. In Eq. (2.3), q_4 is the fourth term of quaternions, \mathbf{q} the vector made of the first three terms and $[q^\wedge]$ the skew symmetric matrix whose elements are from \mathbf{q} .

$$A_{B/N} = (q_4^2 - \mathbf{q}^T \mathbf{q})I + 2\mathbf{q}\mathbf{q}^T - 2q_4[q^\wedge]; \quad (2.3)$$

Two more attitude matrices are used for the ADCS. One is $A_{L/N}$, which rotates a vector from inertial to Local-Vertical-Local-Horizontal reference frame. The Simulink model can take into account any generic orbit, and for the case of a geostationary orbit the only non-identical matrix in Eq. (2.4) is the first one.

$$A_{L/N} = \begin{pmatrix} \cos \theta & \sin \theta & 0 \\ -\sin \theta & \cos \theta & 0 \\ 0 & 0 & 1 \end{pmatrix} \begin{pmatrix} \cos \omega & \sin \omega & 0 \\ -\sin \omega & \cos \omega & 0 \\ 0 & 0 & 1 \end{pmatrix} \begin{pmatrix} 1 & 0 & 0 \\ 0 & \cos i & \sin i \\ 0 & -\sin i & \cos i \end{pmatrix} \begin{pmatrix} \cos \Omega & \sin \Omega & 0 \\ -\sin \Omega & \cos \Omega & 0 \\ 0 & 0 & 1 \end{pmatrix}; \quad (2.4)$$

The other one is $A_{err} = A_B/N A_{req}^T$, which represents the difference between the current pointing and the desired one. When simulating the slew manoeuvre and the reference tracking, $A_{req} = A_L/N$ so $A_{err} = A_{B/L}$. $A_{B/L}$ is a matrix which rotates a vector between body and LVLH frame, such that if it is an identity matrix it means that the satellite is perfectly aligned with the LVLH frame.

2.4 Simulink Model

In this paragraph, the model implemented in Simulink is presented. Other subsystems are nested into the main ones in order to have a neat organization of the workspace. They are placed in a way to make connections more efficient and logical by subject and recurrence of the same variables.

The orbit propagation block contains information regarding the orbit evolution, as well as the eclipse algorithm to check whether the satellite is in umbra, penumbra, or sunlight. The perturbations block contains the different sources of disturbance, with a manual switch to be able to check each of them separately. In the sensors block, a selection logic to switch between gyroscopes and star sensor has been implemented. If the visible stars are less than 2, or ω is above the threshold of $3^\circ/s$, the model utilizes measurements from gyroscopes. In the controller block, a Matlab function, which defines the time instants to switch between the three modes, is implemented. In the actuators block, it is possible to use a manual switch in order to run the simulation either with reaction wheels or thrusters.

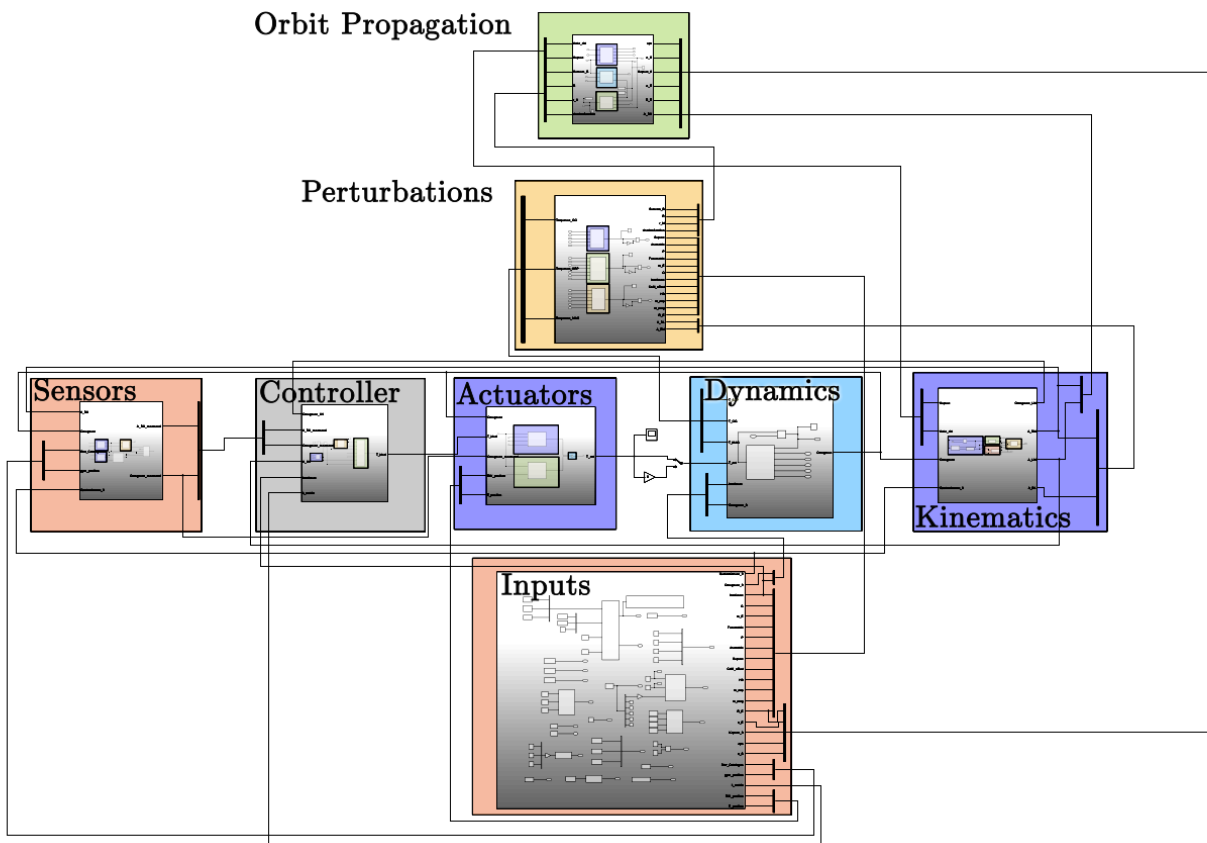


Figure 2.1: Simulink model divided in subsystems

3. Environment Perturbations

Due to the peculiarity of the geostationary orbit, the influence of perturbations is peculiar in itself. Since the orbit has very high altitude, air drag does not play a considerable role in perturbing the nominal attitude, therefore it has not been accounted for. Moreover, there is great amount of time spent in eclipse, which has been considered for SRP perturbation.

3.1 Gravity Gradient

Earth's gravity field does not affect uniformly the entire satellite, owing to the non-symmetrical distribution of mass. For this reason, a torque is generated when the satellite is not in its nominal attitude, where the symmetry axis is aligned with the gravity vector. Consequently, the influence of this perturbation is greater during de-tumbling and slew, while it is nearly zero during reference tracking. The model computes the gravity gradient torque contribution as shown in Eq. (3.1), where r is the spacecraft distance from the Earth center, and the gravitational parameter μ of the Earth is equal to $398600 \text{ km}^3/\text{s}^2$.

$$T_{GG} = \frac{3\mu}{r^3} \hat{r} \times J \hat{r}; \quad (3.1)$$

3.2 Solar Radiation Pressure

The SRP perturbation is due to the solar wind exerting a pressure on the satellite surfaces. First of all, the Sun position with respect to the Earth is needed. SRP only affects the surfaces that are enlightened: this means that the SRP disturbance is null in case of eclipse or for the surfaces that are in shadow. The first condition has been accomplished by checking when the angle between Sun-Earth (\hat{S}) and spacecraft-Earth (\hat{r}) vectors was great enough for the satellite to enter the Earth's shadow cone. Regarding the second case, all forces exerted on a surface are 0 if the dot product between the normal vector of the surface \hat{n}_i and the Spacecraft-Sun vector in body frame \hat{s}_b is negative. ρ_s and ρ_D are respectively the specular and diffuse reflectivities, depending on the surface materials, while P is the average radiation pressure. The center of mass of the satellite is considered with an offset with respect to the geometrical one for the SRP disturbance computation, otherwise the net torque would always be null due to the perfect geometrical and mass symmetry of the preliminary model. The force on each surface is computed as follows.

$$F_i = -PA_i \hat{s}_b \cdot \hat{n}_i \left((1 - \rho_s) \hat{s}_b + 2 \left(\rho_s \hat{s}_b \cdot \hat{n}_i + \frac{1}{3} \rho_D \right) \hat{n}_i \right); \quad T_{SRP} = \sum_{i=1}^{n_{surf}} F_i \times d_{CM,i}; \quad (3.2)$$

While the SRP remains roughly constant for the sunlit part of the orbit, there is a great amount of time the satellite spends in eclipse which must be considered. In order to account for this effect, an eclipse model has been implemented, distinguishing also from umbra and penumbra, as explained below.

3.2.1 Umbra and Penumbra

Penumbra and Umbra regions geometries are modeled as cones, as shown in Fig. 3.1. To evaluate the amount of torque in the penumbra region, a linear gain sh , ranging from 0 to 1, has been applied. 0 corresponds to the umbra region, while 1 corresponds to the sunlit region, with values in between for the penumbra region proportional to the time spent in that part of the orbit [7].

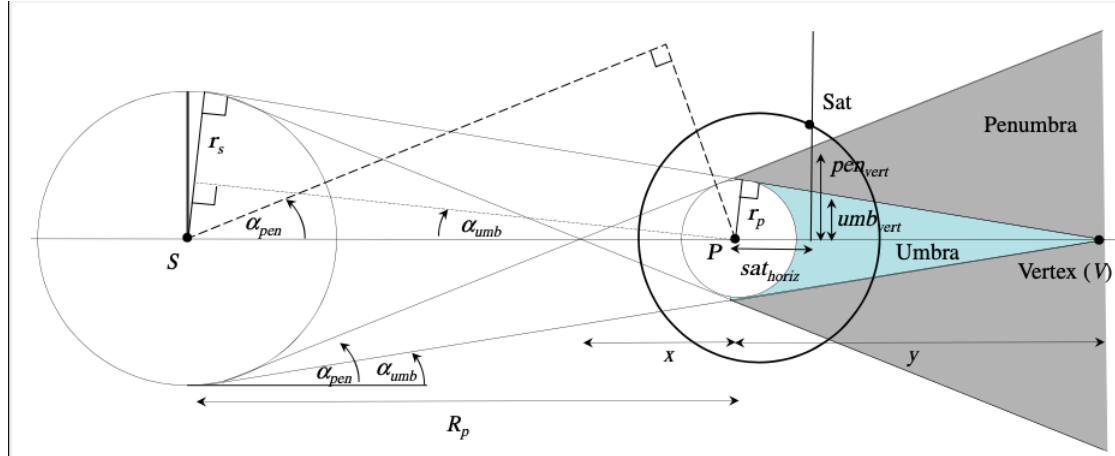


Figure 3.1: Shadow Geometry

Shadow regions are computed implementing an algorithm taken from Vallado [7] and it assumes an instantaneous shadow region change. First, it checks whether the satellite position vector and the sun unit vector are on the same semi-plane, then it checks whether the satellite is within the penumbra cone. If so, it also checks whether the satellite is within the umbra cone. The result of this algorithm is the linear gain, sh , which is multiplied by every force vector, from which the net torque is computed.

3.3 Magnetic Perturbation

The spacecraft has a residual magnetic moment that produces a torque when interacting with the Earth's magnetic field \mathbf{B} . Its model in the inertial frame has been evaluated as stated in Eq. (3.3). Afterwards, the torque acting on the satellite is computed as the cross-product of the residual magnetic moment and \mathbf{B} . The magnetic constants used for the model construction are summarized in Table 3.1.

$$\mathbf{B} = \frac{R_{\oplus} H_0}{r^3} (3(\hat{m} \cdot \hat{r})\mathbf{r} - \hat{m}); \quad T_{mag} = \mathbf{m} \times \mathbf{B}; \quad (3.3)$$

Table 3.1: Magnetic Model Constants

	Value	Symbol
Magnetic Parameter	3.011×10^{-5}	H_0
Earth Magnetic Dipole	$\begin{bmatrix} \sin(11.5^\circ)\cos\Omega_{\oplus}t \\ \sin(11.5^\circ)\sin\Omega_{\oplus}t \\ \cos(11.5^\circ) \end{bmatrix}$	\hat{m}
Earth Angular Velocity	$15^\circ/h$	Ω_{\oplus}

Since the Earth's magnetic field intensity decreases with r , there is a decrement of the magnetic disturbance torque as well. For geostationary orbits, the *dipole model* can be a fairly good approximation of the magnetic perturbation. The magnetic dipole has been selected as $\hat{m} = [0.5; 0.5; 0.5]$ increasing by a margin the average estimate for a worst case scenario condition.

3.4 Disturbance Torques

As shown in Fig. 3.2 and 3.3, for the x and y axes the greatest fluctuations occur in the gravity gradient disturbance, especially during the de-tumbling phase and at the start of the slew maneuver. Furthermore, in the z-axis, the contribution of the SRP disturbance is significantly higher throughout the whole simulation. During the last part of the slew maneuver, the magnitude of the oscillations decreases as the satellite approaches the target attitude.

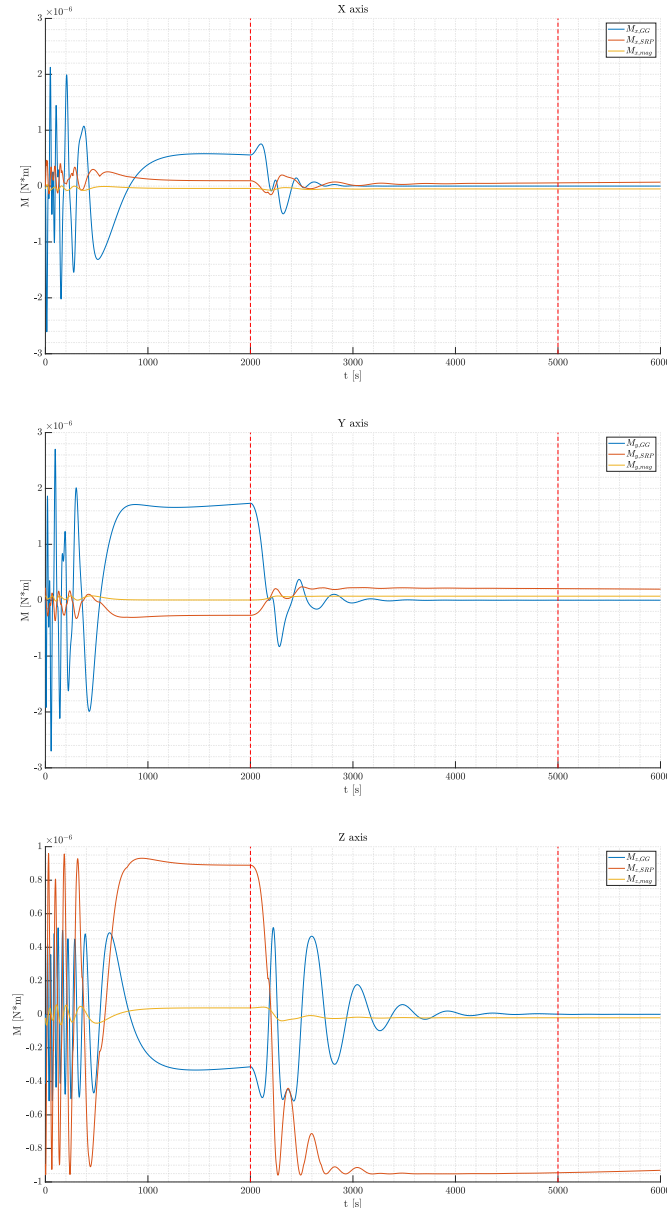
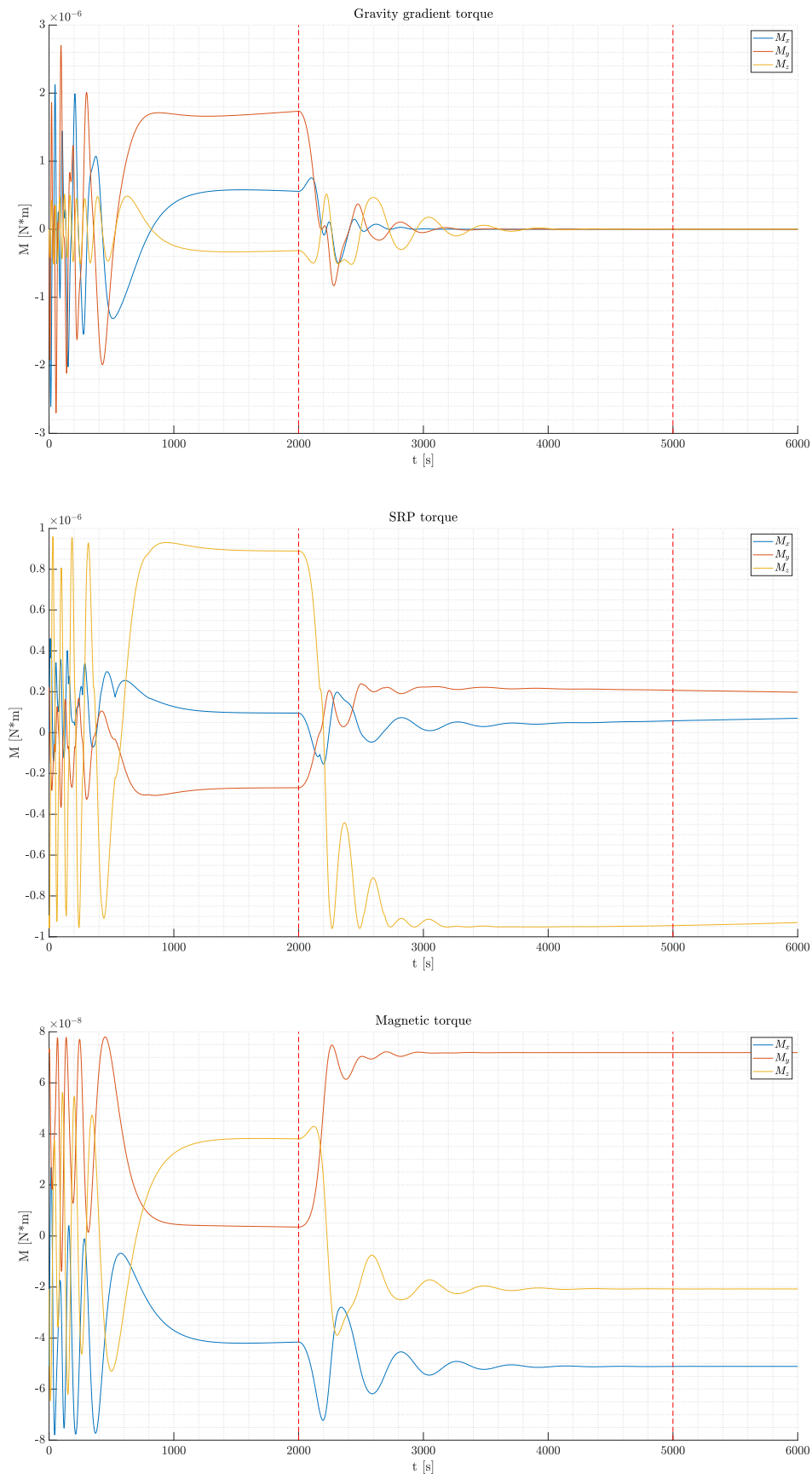


Figure 3.2: Disturbance torques by component

**Figure 3.3:** Disturbance torques by type

4. Sensors

In order to determine the attitude of the spacecraft through the mission phases, multiple attitude sensors have been implemented. Selection of the sensors is based on the project requirements and on the designated mission profile. Gyroscopes were already assigned, however it is feasible and a good choice to add an another sensor in order to have a more robust and accurate system, in case of gyros failure. Since the mission involves a communication satellite that requires precise pointing capabilities, magnetometers were discarded due to low precision characteristics. Additionally, the operational orbit results in significant eclipse periods, hence a sun sensor is not a feasible choice as well. To provide measurements constantly, especially during the tracking phase, a static earth horizon sensor or a star sensor are the best possible options. Due to the mission demands for high precision pointing, a star sensor has been selected.

4.1 Gyroscopes

Gyroscopes have been utilized where the star sensor could not obtain precise measurements, mainly in the de-tumbling and slew maneuver phases. In order to measure all of the angular velocities on the principal axes, three gyroscopes have been placed on the S/C body with no tilt with respect to the already mentioned axes. The angular velocity measured by the sensor was computed as shown in Eq. (4.1).

$$\dot{\omega}_m = \omega + n + b \quad (4.1)$$

Here, ω is the angular velocity of the spacecraft coming from the dynamics. Additionally, n and b represent two *white noise terms*, which are respectively the Angular Random Walk (ARW) and Rate Random Walk (RRW). The variance of the aforementioned noises is computed as defined in Eq. (4.2), which are then fed into the Simulink block "band-limited white noise" by taking their square value.

$$\sigma_n = \frac{ARW}{\sqrt{1/f}}; \quad \sigma_b = \frac{RRW}{\sqrt{1/f}} \quad (4.2)$$

Where f is the sampling frequency. As it is possible to see in Table 4.1, the selected gyroscope for the mission has the following performance properties. Since there is no data regarding the sampling frequency of the ASTRIX 200, 10 Hz is assumed in order to obtain a feasible duration for the simulation execution (7.4).

Table 4.1: Gyroscope Specifications [1]

Model name	Frequency [Hz]	ARW [$^{\circ}/\sqrt{hr}$]	RRW [$^{\circ}/hr^{3/2}$]
ASTRIX 200	10	0.0001	0.00016

4.2 Star Sensor

Due to the mission profile of the satellite, high-accuracy pointing is required. As stated before, this turns into a need for a high-accuracy star sensor as well. The sensor shall be mounted on the top of the satellite, facing upwards, which corresponds to a unit vector in the spacecraft body frame as presented in Eq. (4.3).

$$\mathbf{n}_{ss} = [0 \quad 0 \quad 1]^T \quad (4.3)$$

Star Tracker T1 by TERMA [6] has been selected for the implementation of the star sensor. Its specifications are presented in Table 4.2.

Table 4.2: Star Sensor Specifications

Model name	Frequency [Hz]	σ [arcsec]	FOV [°]	Slew rate [°/s]
T1	10	10	20	3

Noise for the star sensor is implemented introducing an attitude error matrix, which is based on the variance σ of the star sensor. The model is presented in Eq. (4.4):

$$\mathbf{s}_B = A_{sse} A_{B/N} \mathbf{s}_N; \quad (4.4)$$

where A_{sse} is the attitude error matrix due to white noise, $A_{B/N}$ is the matrix coming from the system dynamics, \mathbf{s}_N is the star position in the inertial frame, and \mathbf{s}_B is the measured star position in the spacecraft body frame.

4.2.1 Star Selection

The attitude construction algorithm requires the measurement of at least two stars, which is enough to have a fairly good reconstruction of the S/C attitude. Furthermore, a check on the field of view of the sensor is performed, to ensure the stars are in sight. To increase the possibility to have a star in the field of view, a *star catalog* [5] with 20 stars has been included, with stars ranging from 80° to 90° declination.

4.3 Wahba Attitude Reconstruction

The Wahba Problem is a statistical method to construct the attitude matrix \mathbf{A} from sensor measurements. This matrix is a piece of fundamental information to pass to the control algorithm, which will be explained in chapter 5. As stated before, at least measurements of two stars are needed at any time instant for this method to work. In the GOATS mission, these measurements are provided by the star sensor. The algorithm for the process is explained in these notes [8]. Furthermore, it is necessary to compute the weights, which are based on the precision of all the sensors used, such that the sum of all its elements is 1 as represented in Eq. (4.5).

$$\sum_{i=1}^n \alpha_i = 1 \quad (4.5)$$

Since both of the measurements were taken from the same star sensor, both of the weights were chosen as 0.5.

5. Control

5.1 Lyapunov Controller

A general, non-linear function for attitude control is the Lyapunov controller, which is based on minimising the function V , that reaches 0 value when the desired attitude is achieved. This algorithm fosters the control mode switch just by setting different gains, related to three different modes in which the satellite should be able to operate: de-tumbling, slew manoeuvre, tracking. Before computing the Lyapunov function, it is necessary to retrieve the *attitude error* variables: their objective is to keep track of the difference between the measured attitude position/angular velocity and the required ones.

$$A_{err} = A_{meas} A_{req}^T ; \quad \omega_{err} = \omega_{meas} - A_{err} \omega_{req} ; \quad (5.1)$$

The minimization function used is:

$$V = \frac{1}{2} k_1 \omega_{err}^T J \omega_{err} + 2k_2 \text{tr}(I - A_{err}) ; \quad (5.2)$$

Deriving Eq. (5.2), the ideal control torque is obtained:

$$T_{id} = -k_1 \omega_{err} - k_2 (A_{err}^T - A_{err})^V - J \omega_{meas} \times \omega_{meas} + J (A_{err} \dot{\omega}_{req} - [\omega_{err}]^\wedge A_{err} \omega_{req}) ; \quad (5.3)$$

The parameter k_1 is proportional to the angular velocity error, while k_2 relates to the attitude position error. In this way, it is possible to control the satellite by changing them accordingly to the desired attitude mode. Here, the k_s for the three modes are:

Table 5.1: Controller weights

Mode	k_1	k_2
De-tumbling	5	0
Slew manoeuvre	5	0.1
Tracking	5	0.2

The values for k_s were picked in such a way so that the convergence to zero of ω_{err} would be slower than that of A_{err} . This because otherwise the spacecraft might waste time and resources trying to align itself to the desired direction, while giving preference to nullifying its relative angular velocity. Care has been taken in choosing k_1 to prevent the reaction wheels from saturating, which meant picking a smaller k_1 in order to obtain a weaker control torque to stay within operational bounds.

The controller switches from one mode to the other after a set amount of time, which has been empirically selected as 2000 seconds from the start of the simulation for the switch between de-tumbling and slew, and 5000 seconds from the start of the simulation for the switch between slew and reference tracking.

6. Actuators

The requirements for the mission demanded to use reaction wheels as actuators. These momentum exchange devices were modeled with two separate mechanisms for saturation: one limiting the maximum angular momentum of each spinning wheel, the other limiting the maximum control torque that can be provided. The latter is supposed to indirectly represent the limited torque the electric motors that spin up the wheels can provide. The wheels start with a null angular velocity, changing it according to need. The four wheels are in a pyramidal configuration.

On top of those, thrusters were added to provide redundancy and a way to de-saturate the reaction wheels, should the need arise. In the most recent implementation of the simulation, the reaction wheels never saturate, and as such the thrusters never operate. They were nevertheless modeled and included in the model. The thrusters can be switched on in Simulink, and the results of their implementation are reported in appendix B.

6.1 Reaction Wheels

The working principle of those actuators is based on the acceleration and deceleration of spinning rotors, which are only able to exchange angular momentum with the satellite, but not to produce a net torque. In this study, a set of 4 RWs, organized in a full pyramid configuration, has been considered. The directions of the spin axes of the RWs are represented by the column of the A_{rw} matrix:

$$A_{rw} = \frac{1}{\sqrt{3}} \begin{pmatrix} -1 & +1 & +1 & -1 \\ -1 & -1 & +1 & +1 \\ +1 & +1 & +1 & +1 \end{pmatrix} \quad (6.1)$$

As a feasible option, the RW6000 reaction wheel series [3], has been implemented. The specifications of the RWs have been presented in Table 6.1 :

Table 6.1: Reaction Wheel Specifications

h_{sat} [kgm/s ²]	T_{max} [Nm]
100	0.2

As seen in Fig. 6.1, the RW provides maximum torque up until nearly 300 s for the z-axis. The control required during de-tumbling approaches close to zero around 1200 s and the actuator activates again when the transition to the slew maneuver phase occurs. As the satellite approaches the targeted attitude, required torques reduce in magnitude and approach a near-constant value during the tracking phase. Furthermore, as illustrated in Fig. 6.2, the RW does not reach the saturation limit throughout the whole three phases. Plus, the greatest fluctuations in magnitude are observed at the beginning of the slew maneuver phase. In Fig. 6.3, the angular velocity behavior during the de-tumbling phase

clearly demonstrates the success of the operation as the angular velocities approach zero. Regarding the slew phase, there is a significant increase in angular velocity in the z-axis due to targeted orientation and in the tracking phase it is as the zoomed plot suggests, minimal rotation on the z-axis is sufficient to achieve the tracking.

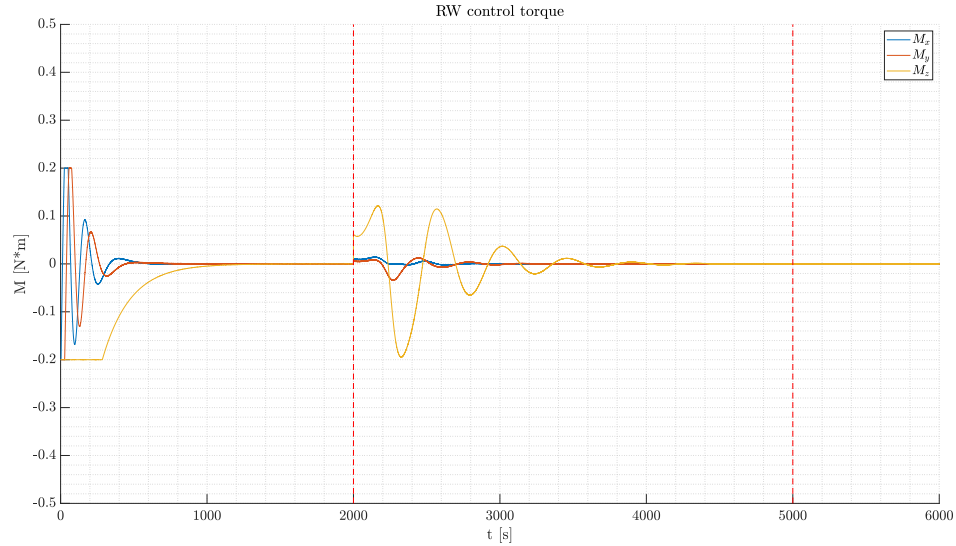


Figure 6.1: Actuator torque for RWs

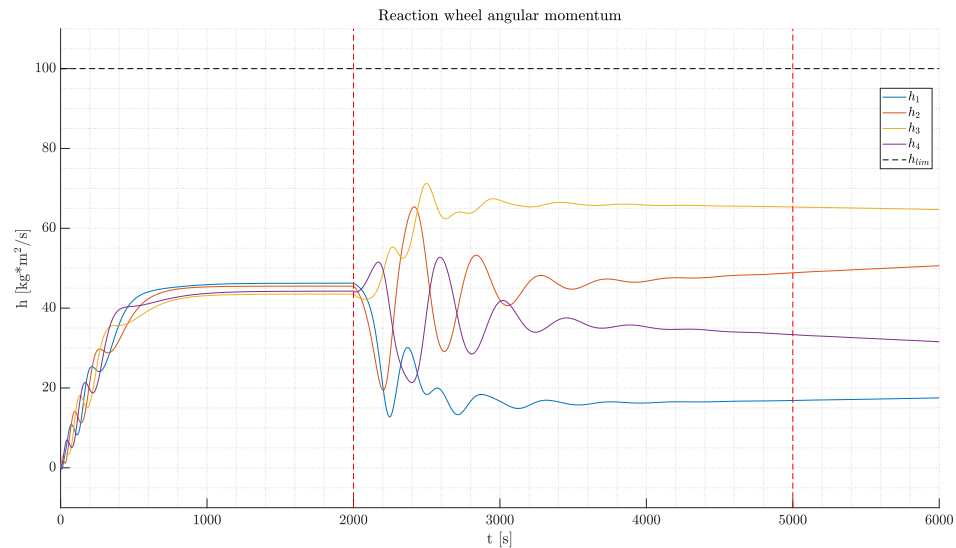


Figure 6.2: Angular momentum for RWs

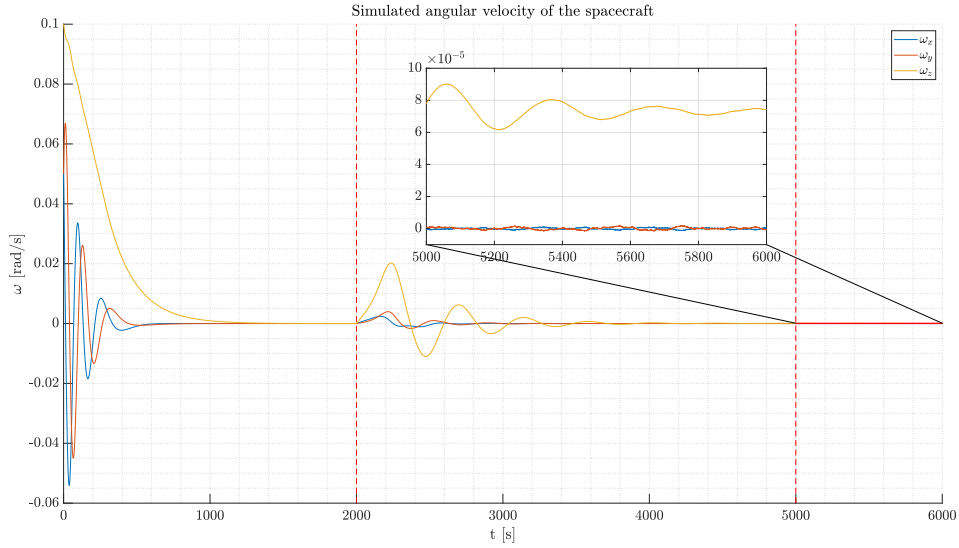


Figure 6.3: Angular velocities with RWs on

6.2 Thrusters

Thrusters are placed in strategical configurations of couples, such that they are able to provide moment torques to the satellite. Since the values of angular velocity are rather small, precision control jet thrusters are needed. An upper bound on the thrust provided $F_{max} = 10 N$ has been selected to comply with specifics of commercial off-the-shelf attitude control thrusters and a lower bound $F_{min} = 0 N$ to impose only positive values. A 4-jet configuration has been selected despite not having a null net thrust to focus the study only on the rotational dynamics.

In order to simulate the model, the first step is to build a matrix containing all the positions of thrusters with respect to the center of mass and another one with unitary thrust directions. The resulting moment and how it is related to the produced torque can be computed as follows:

$$T_{out,T} = \hat{R} F_{out,T}; \quad (6.2)$$

where \hat{R} is reported below in Eq. (6.3).

$$\hat{R} = \begin{pmatrix} lsina & 0 & 0 \\ 0 & lcose & 0 \\ 0 & 0 & xsina - xcosa \end{pmatrix} \begin{pmatrix} 1 & 1 & -1 & -1 \\ -1 & 1 & 1 & -1 \\ 1 & -1 & 1 & -1 \end{pmatrix}; \quad (6.3)$$

On the other hand, $F_{out,T}$ is the thrust produced by each jet at any time step and needs to be defined in order to obtain the actuator torque. The used formula involves the pseudo-inverse matrix of \hat{R} :

$$F_{out,T} = \hat{R}^* T_{ideal} + \gamma\omega; \quad (6.4)$$

where $\gamma\omega$ is a null space vector (made of unitary elements) used to avoid singularities when inverting the matrix \hat{R} .

7. Results

7.1 De-tumbling

During de-tumbling the satellite has to lose all the residual angular velocity acquired during the in-orbit release. Therefore, ω is expected to reach almost a zero value, while no conditions are imposed on the reference attitude. To do so, the S/C controller starts *mode 1* at 0s. Time has arbitrarily been chosen equal to zero at the beginning of this phase. This task can be accomplished with RWs or thrusters as well. Saturation has been taken into account, as it can be seen by the dashed horizontal line.

7.2 Slew Manoeuvre

The scope of this phase is to bring the satellite from one attitude configuration to another. Specifically, the one in which the satellite stops its motion and the desired one: $A_{req} = A_{L/N}$. The pointing error must slew down to zero as well. To do so, the S/C controller starts *mode 2* at 2000s. This value has been selected in order to ensure the residual angular velocities have reached almost zero magnitudes before starting this phase.

7.3 Tracking

This phase starts the operative life of the satellite. After it is completed, the S/C is correctly positioned towards the Earth and it can communicate with on-ground devices. The requirement on satellite attitude is for y and z axis to remain steady, while the x axis needs to move in sync with the orbit. To do so, the S/C controller starts *mode 3* at 5000s. This value has been selected in order to ensure the residual angular velocities have reached almost zero magnitudes after the manoeuvre, and that the pointing error is within a certain threshold before starting this phase.

7.4 Comments on Computational Cost

Since the orbit is geostationary, simulating a full orbit is quite computationally expensive. What affects the simulation the most is the operating frequency of sensors. According to various models, it can be seen that a frequency of 40 Hz is feasible for gyroscopes [8]. However, the computational cost increases drastically for values over 20 Hz, because the sampling frequency directly affects the way noise is generated in the Simulink model. In fact, if the frequency were effectively 40 Hz, it would mean that the model can never take less than 40 steps in a second, as the noise must be sampled at that frequency. This is less noticeable in the first part of the simulation, since the angular velocities are larger, and as such many variables evolve rapidly, forcing the integrator to make even smaller steps. For the scope of this preliminary analysis, the sample frequency of the sensors has been kept at 10 Hz to speed up the computation.

8. Conclusions

The mission objectives have been successfully accomplished with the implementation of the aforementioned manoeuvres of de-tumbling, slew, and reference tracking both by running the model using the RWs and the Thrusters. The results have shown that the attitude errors converge in a fraction of the orbital period, about 5000 seconds, even if the simulation ran for roughly one day.

To improve the simulation further, studies can be made to account for perturbations affecting orbital mechanics; the number of thrusters can be increased in order to provide null net thrust on the satellite; the center of mass can be assumed to have an offset without loss of generality, making it possible to have a decrease of the mass, therefore inertia, over the lifetime of the spacecraft.

Appendix A

Solar panel mass and area computation

Here, the derivation of the mass and area of the solar panel is presented. In Eq. A.1, the total power required from the solar panels, P_{sa} , has been calculated by estimating a power request both in daylight and eclipse with the amount of $P_e = P_d = 800 \text{ W}$, where $\Xi_e = 0.65$ and $\Xi_d = 0.85$ are efficiency factors for eclipse and daylight phases for Direct Energy Transfer (DET), respectively.

$$P_{sa} = \frac{\frac{P_e T_e}{\Xi_e} + \frac{P_d T_d}{\Xi_d}}{T_d} \quad (\text{A.1})$$

Then, the total power generated by the solar arrays per unit area P_{BOL} (at Beginning Of Life) has been calculated in Eq. A.2 by considering the power coming from the Sun, $P_0 = 1358 \text{ W/m}^2$, multiplied by an inherent degradation factor $I_d = 0.6$ and efficiency $\eta = 0.275$ typical for Ga-As solar cells.

$$P_{BOL} = P_0 I_d \eta \quad (\text{A.2})$$

Taking into account the worst case scenario, it's possible to derive the power generated per unit area at the end-of-life, P_{EOL} , with Eq. A.3 by multiplying P_{BOL} with a solar degradation factor L_d .

$$P_{EOL} = P_0 L_d \quad (\text{A.3})$$

Here, L_d computation is reported below in Eq. A.4, considering $d = 0.0375$ and a lifetime of 2 years.

$$L_d = (1 - d)^{\text{lifetime}} \quad (\text{A.4})$$

Finally, the area and mass of the solar array have been calculated in Eqs.A.5 by considering a specific power $P_{spec} = 80 \text{ W/kg}$.

$$A_{sa} = \frac{P_{sa}}{P_{EOL}}; \quad m_{sa} = P_{BOL} \frac{A_{sa}}{P_{spec}}; \quad (\text{A.5})$$

The results are reported below in Table A.1.

Table A.1: Mass and Area of the solar panel result

Parameter	Value
m_{SA}	13.57 Kg
A_{SA}	4.885 m^2

The area of the panels has been divided in two appendages as shown in Fig. 1.2.

Appendix B

Results with thrusters on

In the Simulink model, it is possible to select the actuator to be used thanks to a manual switch. Here, the results obtained running the code using thrusters instead of RWs are reported. In Fig. B.1 the time evolution of the torque provided by the thrusters is presented:

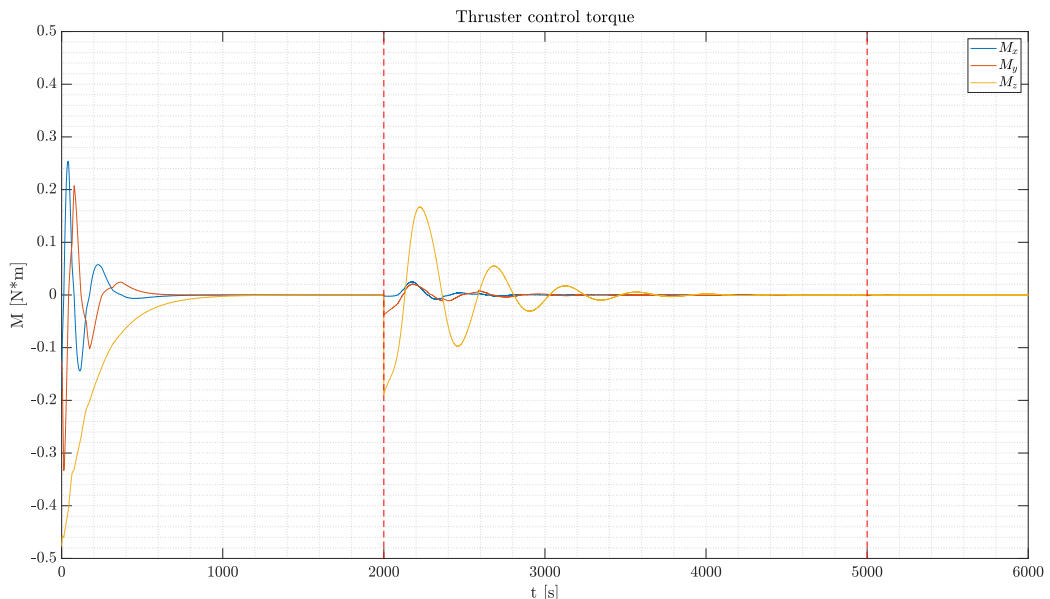


Figure B.1: Angular velocities with thrusters on

while, in Fig. B.2 it is possible to see the plot of the angular velocities of the satellite, with a zoom on the values during the *tracking phase*:

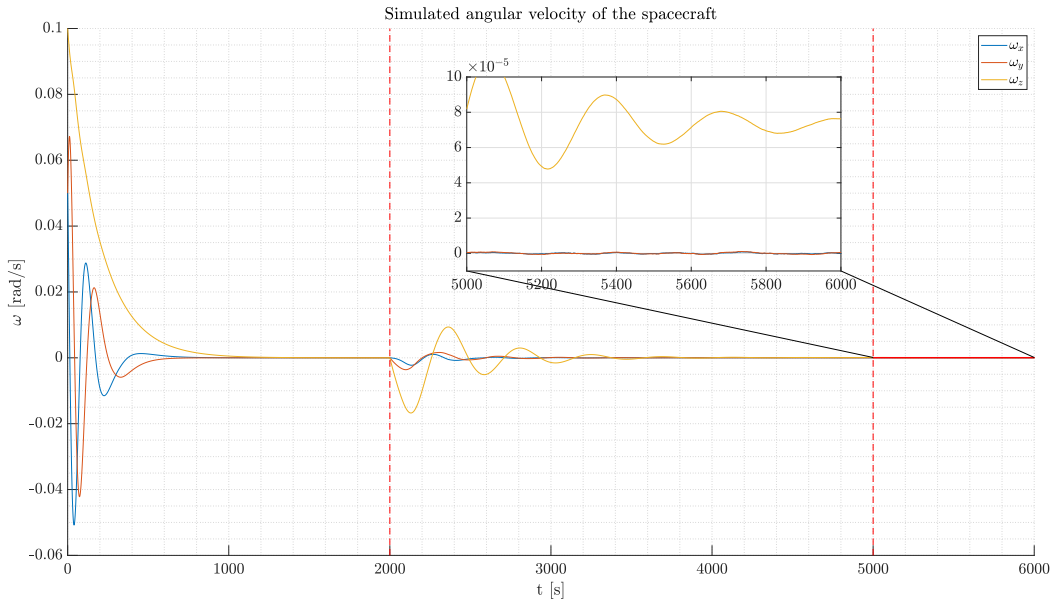


Figure B.2: Angular velocities with thrusters on

Below is an image of the Simulink blocks related to the manual switch acting on the actuators.

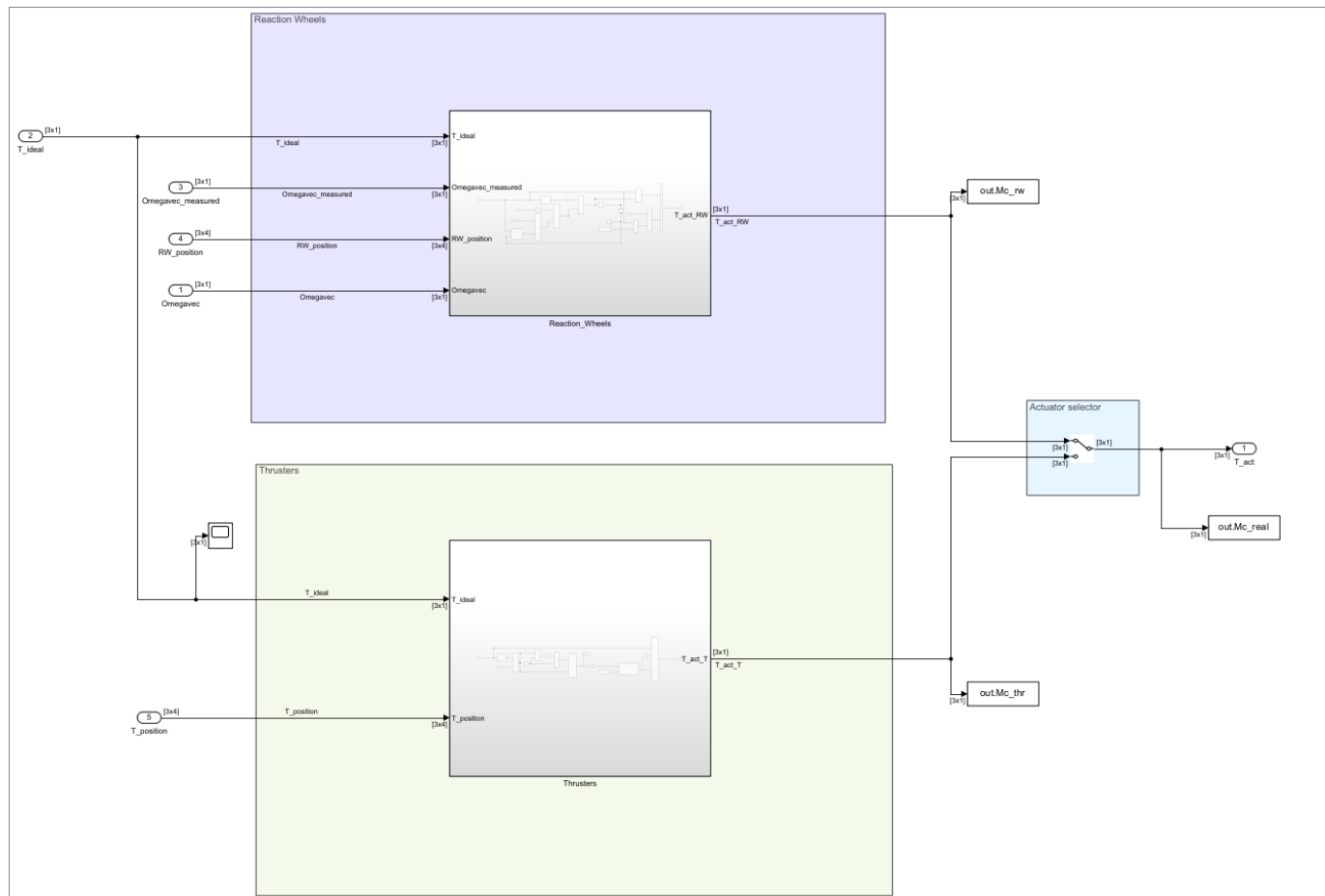


Figure B.3: Manual Switch to select actuators for the simulation

Bibliography

- [1] Airbus. *ASTRIX 200*. URL: <https://www.ixblue.com/wp-content/uploads/2021/12/datasheetastrix200.pdf>.
- [2] *Ariane 5 User's Manual*. URL: <https://www.arianespace.com/wp-content/uploads/2016/10/Ariane5-users-manual-Jun2020.pdf>.
- [3] ESA. *RW6000 Reaction Wheel*. URL: <https://artes.esa.int/projects/rw6000-reaction-wheel>.
- [4] Globalsecurity. *AMOS (Affordable Modular Optimized Satellite)*. URL: <https://www.globalsecurity.org/space/world/israel/amos.htm>.
- [5] David Nash. *The Astronomy Nexus*. URL: <http://astronexus.com/hyg>.
- [6] TERMA. *T1 Star Tracker*. URL: https://www.terma.com/media/pokirm23/2-pager-_t1-star-tracker.pdf.
- [7] David Vallado. "Fundamentals of Astrodynamics and Applications". In: (1997).
- [8] Franco Bernelli Zazzera. *Course notes: Spacecraft Attitude Dynamics*. Tech. rep. Politecnico di Milano, 2020.